Physics Informed Distillation for Diffusion Models

Anonymous authors
Paper under double-blind review

Abstract

Diffusion models have recently emerged as a potent tool in generative modeling. However, their inherent iterative nature often results in sluggish image generation due to the requirement for multiple model evaluations. Recent progress has unveiled the intrinsic link between diffusion models and Probability Flow Ordinary Differential Equations (ODEs), thus enabling us to conceptualize diffusion models as ODE systems. Simultaneously, Physics Informed Neural Networks (PINNs) have substantiated their effectiveness in solving intricate differential equations through implicit modeling of their solutions. Building upon these foundational insights, we introduce Physics Informed Distillation (PID), that employs a student model to represent the solution of the ODE system corresponding to the teacher diffusion model, akin to the principles employed in PINNs. Through experiments on CIFAR 10 and ImageNet 64x64, we observe that PID attains performance comparable to recent distillation methods. Notably, it demonstrates predictable trends concerning method-specific hyperparameters and eliminates the need for synthetic dataset generation during the distillation process. Both of which contribute to its easy-to-use nature as a distillation approach for Diffusion Models.

1 Introduction

Diffusion models (Sohl-Dickstein et al., 2015; Song et al., 2020b; Ho et al., 2020) have demonstrated remarkable performance in various tasks, including image synthesis (Dhariwal & Nichol, 2021; Nichol et al., 2021; Ramesh et al., 2022; Saharia et al., 2022a), semantic segmentation (Baranchuk et al., 2021; Wolleb et al., 2022; Kirillov et al., 2023), and image restoration (Saharia et al., 2022b; Whang et al., 2022; Li et al., 2022; Niu et al., 2023). With a more stable training process, it has achieved better generation results that outperform other generative models, such as GAN (Goodfellow et al., 2020), VAE (Kingma & Welling, 2013), and normalizing flows (Kingma & Dhariwal, 2018). The success of diffusion models can mainly be attributed to their iterative sampling process which progressively removes noise from a randomly sampled Gaussian noise. However, this iterative refinement process comes with the huge drawback of low sampling speed, which strongly limits its real-time applications (Salimans & Ho, 2022; Song et al., 2023).

Recently, Song et al. (2021) and Karras et al. (2022) have proposed viewing diffusion models from a continuous time perspective. In this view, the forward process that takes the distribution of images to the Gaussian distribution can be viewed as a stochastic differential equation (SDE). On the other hand, diffusion models learn the associated backward SDE through score matching. Interestingly, Song et al. (2021) demonstrate that diffusion models can also be used to model a probability flow ODE system that is equivalent in distribution to the marginal distributions of the SDE. In addition, Physics Informed Neural Networks (PINNs) have proven effective in solving complex differential equations (Raissi et al., 2019; Cuomo et al., 2022) by learning the underlying dynamics and relationships encoded in the equations.

Building upon these developments, we propose a distillation method for diffusion models called Physics Informed Distillation (PID), a method that takes a PINNs-like approach to distill a single-step diffusion model. Our method trains a model to predict the trajectory at any point in time given the initial condition relying solely on the ODE system. During training, we view the teacher diffusion model as an ODE system to be solved by the student model in a physics-informed fashion. In this framework, the student model

approximates the ODE trajectories, as illustrated in Figure 1, without explicitly observing the images in the trajectory. In detail, our contributions can be summarized as follows:

- We propose Physics Informed Distillation (PID), a knowledge distillation technique heavily inspired by PINNs that enables single-step image generation.
- We analyze Physics Informed Distillation (PID), providing theoretical bounds for the method.
- Through experiments on CIFAR-10 and ImageNet 64x64, we showcase our approaches' effectiveness in generating high-quality images with only a single forward pass.
- We demonstrate that similar to PINNs where the performance improvements saturate at a sufficiently large number of collocation points, our approach with a high enough discretization number performs best, showcasing its potential as a knowledge distillation approach that does not need additional tuning of method specific hyperparameters.

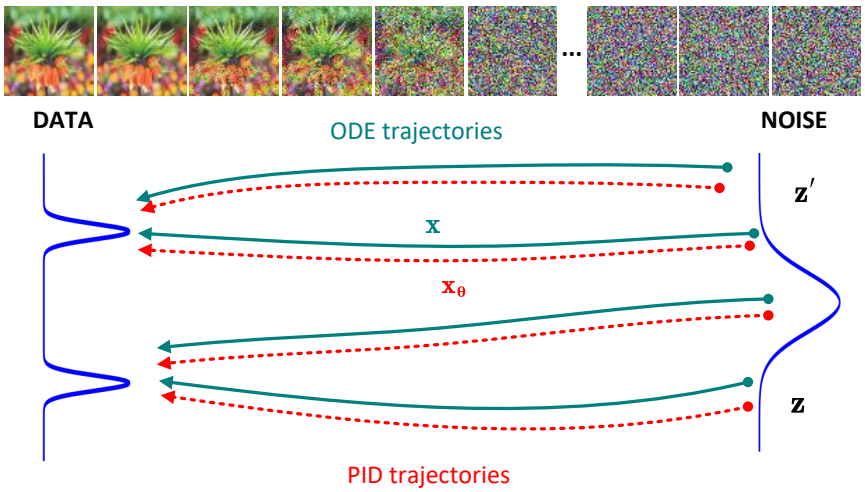

Figure 1: An overview of the proposed method, which involves training a model $\mathbf{x}_\theta(\mathbf{z}, \cdot)$ to approximate the true trajectory $\mathbf{x}(\mathbf{z}, \cdot)$.

2 Related Works

The remarkable performance of diffusion models in various image generation tasks has garnered considerable attention. Nevertheless, the slow sampling speed associated with these models remains a significant drawback. Consequently, researchers have pursued two primary avenues of exploration to tackle this challenge: training-free and training-based methods.

Training-free methods. Several training-free methods have been proposed in the field of diffusion model research to expedite the generation of high-quality images. Notably, Lu et al. (2022) introduced DPM-Solver, a high-order solver for diffusion ODEs. This method significantly accelerates the sampling process of diffusion probabilistic models by analytically computing the linear part of the solution. With only ten steps, DPM-Solver achieves decent performance compared to the usual requirement of hundreds to thousands of function evaluations. Another noteworthy approach is DEIS (Zhang & Chen, 2022), which exploits the semilinear structure of the empirical probability flow ODE, as in DPM-Solver, to enhance sampling efficiency. These methods demonstrate the surprising ability to significantly reduce the number of model evaluations while remaining training-free. However, it is important to note that they only mitigate the core issue of the iterative sampling nature of diffusion models without eliminating it entirely. In contrast to these training-free methods, training-based approaches have been proposed to perform single-step inference while aiming

to maintain the performance of the teacher diffusion model. Our paper focuses on this particular field of study.

Training-based methods. In the domain of diffusion model distillation, training-based strategies can be broadly classified into two primary groups: those relying on synthetic data and those trained with original data. Among the former, noteworthy methods such as Knowledge Distillation (Luhman & Luhman, 2021), DSNO (Zheng et al., 2022), and Rectified Flow (Liu et al., 2022) have recently exhibited their efficacy in distilling single-step student models. However, a notable drawback inherent in these approaches is the computationally costly nature of generating such synthetic data, which presents scalability challenges, particularly for larger models. In response, methods using only the original dataset such as Salimans & Ho (2022) (Progressive Distillation) and Song et al. (2023) (Consistency Models) have emerged as solutions to this issue. Progressive Distillation adopts a multi-stage distillation approach, while Consistency Models employ a self-teacher model, reminiscent of self-supervised learning techniques. Another noteworthy mention is the recent data-free distillation approach BOOT (Gu et al., 2023) which only requires a teacher model without any synthetic data similar to our proposed approach.

3 Preliminaries

3.1 Diffusion Models

Physics Informed Knowledge Distillation is heavily based on the theory of continuous time diffusion models by Song et al. (2021). These models describe the dynamics of a diffusion process through a stochastic differential equation:

$$\mathrm{d}\mathbf{x} = \mathbf{f}(\mathbf{x}, t)\mathrm{d}t + g(t)\mathrm{d}\boldsymbol{w}_t, \tag{1}$$

where $t \in [0, T]$, $\boldsymbol{w}_t$ is the standard Brownian motion (Uhlenbeck & Ornstein, 1930; Wang & Uhlenbeck, 1945) (a.k.a Wiener process), $\mathbf{f}(\cdot, \cdot)$ and $g(\cdot)$ denote the drift and diffusion coefficients, respectively. The distribution of $\mathbf{x}$ is denoted as $p_t(\mathbf{x})$ with the initial distribution $p_0(\mathbf{x})$ corresponding to the data distribution, p_{data}.

As proven in Song et al. (2021), this diffusion process has a corresponding probability flow ODE with the same marginal distributions $p_t(\mathbf{x})$ of the form:

$$\mathrm{d}\mathbf{x} = \left[\mathbf{f}(\mathbf{x}, t) - \frac{1}{2}g(t)^2\nabla_{\mathbf{x}} \log p_t(\mathbf{x})\right] \mathrm{d}t, \tag{2}$$

where $\nabla_{\mathbf{x}} \log p_t(\mathbf{x})$ denotes the score function. Diffusion models learn to generate images through score matching (Song et al., 2020b), approximating the score function as $\nabla_{\mathbf{x}} \log p_t(\mathbf{x}) \approx \mathbf{s}_\phi(\mathbf{x}, t)$ with $\mathbf{s}_\phi(\mathbf{x}, t)$ being the score model parameterized by ϕ. As such, diffusion models learn to model the probability flow ODE system of the data while relying on iterative finite solvers to approximate the modeled ODE.

3.2 Physics Informed Neural Networks (PINNs)

PINNs are a scientific machine-learning technique that can solve any arbitrary known differential equation (Raissi et al., 2019; Cuomo et al., 2022). They rely heavily on the universal approximation theorem (Hornik et al., 1989) of neural networks to model the solution of the known differential equation (Cuomo et al., 2022). To better explain the learning scheme of PINNs, let us first consider an ODE system of the form:

$$\begin{aligned} \frac{\mathrm{d}\mathbf{x}}{\mathrm{d}t} &= u(\mathbf{x}, t), \\ \mathbf{x}(T) &= x_0, \end{aligned} \tag{3}$$

where $t \in [0, T]$, $u(\cdot, \cdot)$ is an arbitrary continuous function and x_0 is an arbitrary initial condition at the time T. To solve this ODE system, Physics Informed Neural Networks (PINNs) can be divided into two distinct approaches: a soft conditioning approach (Cuomo et al., 2022), in which boundary conditions are sampled and trained, and a hard conditioning approach, (Lagaris et al., 1998; Cuomo et al., 2022) where such

conditions are automatically satisfied through the utilization of skip connections. For the sake of simplicity, we exclusively focus on the latter easier approach, where the PINNs output is represented as follows:

$$\begin{aligned} \mathbf{x}_\theta(t) &= c_{\text{skip}}(t)x_0 + c_{\text{out}}(t)\mathbf{X}_\theta(t), \\ \text{where } c_{\text{skip}}(T) &= 1 \text{ and } c_{\text{out}}(T) = 0, \end{aligned} \tag{4}$$

here $\mathbf{X}_\theta$ denotes a neural network parametrized by θ and the functions, c_{skip} and c_{out}, are chosen such that the boundary condition is always satisfied. Following this, PINNs learn by reducing the residual loss denoted as:

$$\mathcal{L} = \| \frac{\mathrm{d}\mathbf{x}_\theta(t)}{\mathrm{d}t} - u(\mathbf{x}_\theta(t), t)\|^2. \tag{5}$$

Through this, they can model physical phenomena represented by such ODE systems. Inspired by PINNs ability to solve complex ODE systems (Lagaris et al., 1998; Cuomo et al., 2022), we use a PINNs-like approach to perform Physics Informed Distillation. This distillation approach uses the residual loss in PINNs to solve the probability flow ODE system modeled by diffusion models. Through this distillation, the student trajectory function in Figure 1 can perform fast single-step inference by querying the end points of the trajectory.

4 Physics Informed Knowledge Distillation

4.1 Trajectory Functions

In this section, we begin by introducing the concept of trajectory functions, representing solutions to a given arbitrary ODE system. Subsequently, we demonstrate how these trajectory functions can be learned through the application of a simple PINNs loss, resulting in a single-step sampler. It's noteworthy that a recent work, BOOT, also employs a PINNs-like approach to distill trajectory functions. However, their primary focus is on distilling the Signal ODE, while our emphasis lies in the direct distillation of the probability flow ODE. Later sections will delve into specific modifications, highlighting challenges encountered and successful adaptations made to effectively distill the probability flow ODE.

From this point onwards, we adopt the configuration introduced in EDM (Karras et al., 2022). The configuration utilizes the empirical probability flow ODE on the interval $t \in [\epsilon, T]$ of the following form:

$$\begin{aligned} \frac{\mathrm{d}\mathbf{x}}{\mathrm{d}t} &= -t\mathbf{s}_\phi(\mathbf{x}, t) \\ &= \frac{\mathbf{x} - D_\phi(\mathbf{x}, t)}{t}, \end{aligned} \tag{6}$$

where $\mathbf{x}(T) \sim \mathcal{N}(\mathbf{0}, T^2\mathbf{I})$, $\epsilon = 0.002$, $T = 80$ and $D_\phi(\mathbf{x}, t)$ is the teacher diffusion model. Under the assumption that Diffusion Models are Lipschitz continuous on the given time interval, this ODE system exhibits a unique solution (Grant, 1999). As such, we can conceptualize each noise as having its uniquely associated trajectory function, as illustrated in Figure 1. We denote this trajectory function as $\mathbf{x}(\mathbf{z}, t)$, where $\mathbf{z}$ represents the noise's initial condition at time T. Our objective is to train a model $\mathbf{x}_\theta(\mathbf{z}, t)$ that precisely captures the actual trajectories $\mathbf{x}(\mathbf{z}, t)$ for any arbitrary noise, $\mathbf{z}$. To achieve this, we adopt a PINNs-like approach to learn the trajectory functions $\mathbf{x}(\mathbf{z}, t)$. Specifically, we can minimize the residual loss, similar to the methodology employed in PINNs.

Similar to in PINNs, we require our solution function, $\mathbf{x}_\theta(\cdot, \cdot)$, to satisfy the boundary condition $\mathbf{x}_\theta(\mathbf{z}, T) = \mathbf{z}$. In PINNs literature, the two common approaches to achieve this is either by using a soft condition (Cuomo et al., 2022), in which boundary conditions are sampled and trained or through a strict condition (Lagaris et al., 1998) where these conditions are arbitrarily satisfied using skip connections. Since the use of skip connections is also common in diffusion training (Karras et al., 2022), we take inspiration from both fields and parametrize our model as:

$$\begin{aligned} &\mathbf{x}_\theta(\mathbf{z}, t) = c_{\text{skip}}(t)\ \mathbf{z} + c_{\text{out}}(t)\ \mathbf{X}_\theta\left(c_{\text{in}}(T)\ \mathbf{z}, c_{\text{noise}}(t)\right), \\ &\text{where } c_{\text{skip}}(t) = \frac{t}{T}, c_{\text{out}}(t) = \frac{T-t}{T}, c_{\text{in}}(T) = \frac{1}{\sqrt{0.5^2 + T^2}} \text{ and } c_{\text{noise}}(t) = \frac{\ln t}{4}. \end{aligned} \tag{7}$$

Here, $\mathbf{X}_\theta$ denotes the neural network to be trained(insight into the choice of skip connection functions are provided in Appendix A.2.) Using the vanilla PINNs loss on the probability flow ODE, the loss is given as:

$$\mathcal{L}_{\text{PINNs}} = \mathbb{E}_{i,\mathbf{z}}\left[d\left(\frac{\mathrm{d}\mathbf{x}_\theta(\mathbf{z},t_i)}{\mathrm{d}t_i}, \frac{\mathbf{x}_\theta(\mathbf{z},t_i) - D_\phi\left(\mathbf{x}_\theta(\mathbf{z},t_i),t_i\right)}{t_i}\right)\right] \tag{8}$$

where $d(\cdot,\cdot)$ is any arbitrary distance metric (e.g. L2 and LPIPS). In diffusion models, the Lipschitz constant of the ODE systems they model tend to explode to infinity near the origin (Yang et al., 2023). For instance, in Equation 6, it can be seen that the ODE system explodes as t approaches 0. Consequently, training a solver in a vanilla physics informed fashion may yield suboptimal performance, as it involves training the gradients of our student model to correspond with an exploding value. To alleviate this, we shift the variables as:

$$\mathcal{L}_{\text{PINNs}} = \mathbb{E}_{i,\mathbf{z}}\left[d\left(\mathbf{x}_\theta(\mathbf{z},t_i) - t_i\frac{\mathrm{d}\mathbf{x}_\theta(\mathbf{z},t_i)}{\mathrm{d}t_i}, D_\phi\left(\mathbf{x}_\theta(\mathbf{z},t_i),t_i\right)\right)\right]. \tag{9}$$

Through this, we can obtain a stable training loss that does not explode when time values near the origin are sampled. By performing this straightforward variable manipulation, we can interpret the residual loss as the process of learning to match the composite student model, parametrized by θ, on the left portion of the distance metric with the output of the teacher diffusion model on the right portion of the distance metric. Since the output of the teacher diffusion model on the right is also dependent on the student model, we can also view this from a self-supervised perspective. In this perspective, it is often conventional to stop the gradients flowing from the teacher model (Grill et al., 2020; Caron et al., 2021; Chen et al., 2020). In line with this, we also stop the gradients flowing from the teacher diffusion model during training.

4.2 Numerical Differentiation

In what follows, we will briefly overview the challenges associated with automatic differentiation for gradient computation. Then, we propose the adoption of numerical differentiation, a technique prevalent in standard PINNs training and also employed in the BOOT framework.

The residual loss in PINNs requires computing gradients of the trajectory function with respect to its inputs, which can be computationally expensive using forward-mode backpropagation and may not be readily available in certain packages. Furthermore, studies such as Chiu et al. (2022) have demonstrated that training PINNs using automatic differentiation can lead to convergence to unphysical solutions. To address these challenges, we employ a different approach by relying on a straightforward numerical differentiation method to approximate the gradients. Specifically, we utilize a first-order upwind numerical approximation, given as:

$$\frac{\mathrm{d}\mathbf{x}_\theta(\mathbf{z},t)}{\mathrm{d}t}_{\text{num}} = \frac{\mathbf{x}_\theta(\mathbf{z},t) - \mathbf{x}_\theta(\mathbf{z},t-\Delta t)}{\Delta t}\,. \tag{10}$$

By employing this numerical differentiation scheme, we can efficiently estimate the gradients needed for the training process. This approach offers a simpler alternative to costly forward-mode backpropagation and mitigates the issues related to convergence to unphysical solutions observed in automatic differentiation-based training of PINNs.

4.3 Physics Informed Distillation

In this section, we consolidate the insights gathered from the preceding sections to present Physics Informed Distillation (PID) as a distillation approach for single-step sampling. In addition, we conduct a theoretical analysis of our proposed PID loss, establishing bounds on the generation error of the distilled PID student model.

Replacing the exact gradients with the proposed numerical differentiation and setting $\Delta t = t_i - t_{i+1}$, we obtain the Physics Informed Distillation loss:

$$\mathcal{L}_{\text{PID}} = \mathbb{E}_{i,\mathbf{z}}\left[d\left(\mathbf{x}_\theta(\mathbf{z},t_i) - t_i\frac{\mathbf{x}_\theta(\mathbf{z},t_i) - \mathbf{x}_\theta(\mathbf{z},t_{i+1})}{t_i - t_{i+1}}, \mathrm{sg}\left(D_\phi(\mathbf{x}_\theta(\mathbf{z},t_i),t_i)\right)\right)\right] \tag{11}$$

Algorithm 1 Physics Informed Distillation Training

Input: Trained teacher model D_ϕ, PID model $\mathbf{x}_\theta$, LPIPS loss $d(\cdot,\cdot)$, learning rate η, discretization number N.

$\theta \leftarrow \phi$ // Initialize student from teacher
repeat
  $i \sim U[0, 1, ..., N]$ // Sample time index from a uniform distribution
  $\mathbf{z} \sim \mathcal{N}(\mathbf{0}, T^2\mathbf{I})$ // Sample data
  $\frac{\mathrm{d}\mathbf{x}}{\mathrm{d}t} \leftarrow (\mathbf{x}_\theta(\mathbf{z}, t_i) - \mathbf{x}_\theta(\mathbf{z}, t_{i+1}))/(t_i - t_{i+1})$ // Numerical gradient approximation
  $\mathbf{x}_{\text{teacher}} \leftarrow \text{sg}\left(D_\phi\left(\mathbf{x}_\theta(\mathbf{z}, t_i), t_i\right)\right)$ // Get teacher model output
  $\mathcal{L}_{\text{PID}} \leftarrow d\left(\mathbf{x}_{\text{teacher}}, \mathbf{x}_\theta(\mathbf{z}, t_i) - t_i * \frac{\mathrm{d}\mathbf{x}}{\mathrm{d}t}\right)$ // Loss calculation according to Equation 11
  $\theta \leftarrow \theta - \eta\nabla_\theta\mathcal{L}_{\text{PID}}$ // Update weights
until model converged

where $\text{sg}(\cdot)$ denotes the stop gradient operation. For the time-space discretization scheme, we follow the same scheme as in EDM (Karras et al., 2022). We choose the LPIPS distance metric motivated by Rectified Flow Distillation (Liu et al., 2022) and Consistency Model's (Song et al., 2023) recent successes with this metric. The discretization error added in such a scheme is bounded as shown in the Theorem 1.

Theorem 1. *Assuming $D_\phi(\mathbf{x}, t)$ is Lipchitz continuous with respect to $\mathbf{x}$, if $\mathcal{L}_{PID} = 0$, $||\mathbf{x}_\theta(\mathbf{z}, t) - \mathbf{x}(\mathbf{z}, t)||_2 \leq \mathcal{O}(\Delta t)$, where $\Delta t = \max_{i\in[0,N-1]} |t_{i+1} - t_i|$.*

Proof. When $\mathcal{L}_{\text{PID}}$ loss goes to 0, since the distance metric has the property,

$$x = y \iff d(x, y) = 0. \tag{12}$$

We have the following equality $\forall \mathbf{z} \sim \mathcal{N}(\mathbf{0},\, T^2\mathbf{I}), \forall i \in [0, 1, ..., N-2]$,

$$\begin{aligned}
\mathbf{x}_\theta(\mathbf{z}, t_i) - t_i \frac{\mathbf{x}_\theta(\mathbf{z}, t_i) - \mathbf{x}_\theta(\mathbf{z}, t_{i+1})}{t_i - t_{i+1}} &= D_\phi(\mathbf{x}_\theta(\mathbf{z}, t_i), t_i) \\
\Delta t_i \mathbf{x}_\theta(\mathbf{z}, t_i) - t_i \mathbf{x}_\theta(\mathbf{z}, t_i) + t_i \mathbf{x}_\theta(\mathbf{z}, t_{i+1}) &= \Delta t_i D_\phi(\mathbf{x}_\theta(\mathbf{z}, t_i), t_i) \text{ where } \Delta t_i = |t_{i+1} - t_i| \\
\mathbf{x}_\theta(\mathbf{z}, t_{i+1}) &= \mathbf{x}_\theta(\mathbf{z}, t_i) - \Delta t_i \frac{-D_\phi(\mathbf{x}_\theta(\mathbf{z}, t_i), t_i)}{t_i}
\end{aligned} \tag{13}$$

Since this equality holds $\forall \mathbf{z} \sim \mathcal{N}(\mathbf{0},\, T^2\mathbf{I}), \forall i \in [0, 1, ..., N-2]$, the trajectory model $\mathbf{x}_\theta(\mathbf{z}, t_i)$ will have equivalent trajectories as that obtained through a euler solver. As such, it will have the same discretization error bound, $\mathcal{O}(\Delta t)$.

□

An intriguing aspect of this theorem lies in its connection to Euler solvers and first-order numerical gradient approximations. Specifically, when our model achieves a loss of 0, the approximate trajectories traced by the PID-trained model, denoted as $\mathbf{x}_\theta(\mathbf{z}, t)$, effectively mirrors those obtained using a simple Euler solver employing an equivalent number of steps, denoted as N. Moreover, as indicated in Theorem 1, the discretization error is well controlled and diminishes with an increasing number of discretization steps, N. This observation suggests that by employing a higher number of discretization steps, we can effectively minimize the error associated with the discretization process, achieving improved performance.

By employing the PID training scheme, the resulting model can effectively match the trajectory function $\mathbf{x}(\mathbf{z}, t)$ within the specified error bound mentioned earlier. Single-step inference can be performed by simply querying the value of the approximate trajectory function $\mathbf{x}_\theta(\mathbf{z}, t)$ at the endpoint ϵ, $\mathbf{x}_\theta(\mathbf{z}, \epsilon)$. With this, we observe that by treating the teacher diffusion model as an ODE system, we can theoretically train a student model to learn the trajectory function up to a certain discretization error bound without data and perform fast single-step inference. Algorithm 1 provides the pseudo-code describing our Physics Informed Distillation training process. After training, single-step generation can be achieved by querying the learned trajectory functions at the origin, denoted as $\mathbf{x}_\theta(\mathbf{z}, t_{min})$.

5 Results

In this section, we empirically validate our theoretical findings through various experiments on CIFAR-10 (Krizhevsky & Hinton, 2009) and ImageNet 64x64 (Deng et al., 2009). The results are compared according to Frechet Inception Distance (FID) (Heusel et al., 2017b) and Inception Score (IS) (Salimans et al., 2016). All experiments for PID were initialized with the EDM teacher model. In addition, unless stated otherwise, a discretization of 250 and LPIPS metric was used during training. More information on the training details can be seen in Appendix A.1.

Table 1: FID and IS table comparisons for various sampler based and distillation based methods on CIFAR-10. The asterisk (*) denotes methods that require the generation of synthetic dataset. The neural function evaluations (NFE), FID score and IS values reported where obtained from the respective papers.

METHOD	NFE (↓)	FID (↓)	IS (↑)
EDM (Karras et al., 2022)	36	2.04	
EDM+Euler Solver (Karras et al., 2022)	250	2.10	
DDPM Ho et al. (2020)	1000	3.17	9.46
DDIM (Song et al., 2020a)	10	13.36	
	50	4.67	
DPM-Solver-Fast (Lu et al., 2022)	10	4.70	
3-DEIS (Zhang & Chen, 2022)	10	4.17	
Teacher DDPM			
Progressive Distillation (Salimans & Ho, 2022)	1	8.34	8.69
DSNO* (Zheng et al., 2022)	1	3.78	-
Teacher Rectified Flow			
2-Rectified Flow (+ distill)* (Liu et al., 2022)	1	4.85	9.01
Teacher EDM			
Consistency Model (Song et al., 2023)	1	3.55	9.48
BOOT (Gu et al., 2023)	1	4.38	-
Diff-Instruct (Luo et al., 2023)	1	4.12	9.89
Equilibrium Models (Geng et al., 2023)	1	6.91	9.16
PID (Ours)	1	**3.92**	**9.13**

Table 2: FID table comparisons for various distillation based methods on ImageNet 64x64. The asterisk (*) denotes methods that require the generation of a synthetic dataset.

Method	NFE (↓)	FID (↓)
ADM (Dhariwal & Nichol, 2021)	250	2.07
EDM (Karras et al., 2022)	79	2.44
EDM+Euler Solver (Karras et al., 2022)	250	2.41
BigGAN-deep (Brock et al., 2019)	1	4.06
Teacher DDPM		
Progressive Distillation (Salimans & Ho, 2022)	1	15.39
DSNO* (Zheng et al., 2022)	1	7.83
Teacher EDM		
Consistency Model (Song et al., 2023)	1	6.20
BOOT (Gu et al., 2023)	1	12.3
Diff-Instruct (Luo et al., 2023)	1	4.24
PID (Ours)	1	**9.49**

We quantitatively compare the sample quality of our PID for diffusion models with other training-free and training-based methods for diffusion models, including DSNO (Zheng et al., 2022), Rectified Flow (Liu et al., 2022), PD (Salimans & Ho, 2022), CD (Song et al., 2023), BOOT (Gu et al., 2023) and Diff-Instruct (Luo et al., 2023). In addition to the baseline EDM (Karras et al., 2022) model, we make comparisons with other sampler-based fast generative models, such as DDIM (Song et al., 2020a), DPM-solver (Lu et al., 2022), and DEIS (Zhang & Chen, 2022). In Table 1 we show our results on CIFAR 10 dataset. In this, PID maintains a competitive result in both FID and IS with the most recent single-step generation methods, achieving an FID of 3.92 and IS of 9.13, while outperforming a few. In particular, we outperform Diff-Instruct, Rectified Flow, PD, Equilibrium Models and BOOT by a decent margin on CIFAR-10. On the other hand, we maintain a competitive performance with DSNO and CD, only losing to it by a small margin.

(a) Random samples from EDM (b) Random samples from PID

Figure 2: Conditional image generation comparison on ImageNet 64×64 for the same seed with the same class label "Siberian husky". Left panel: random samples generated by teacher model EDM. Right panel: generated by student PID model.

Table 2 presents the results obtained from experiments conducted on ImageNet 64x64. Analyzing Table 2, we observe that our method surpasses PD (Salimans & Ho, 2022), achieving an FID of 9.49. Nevertheless, echoing our observations from the CIFAR-10 experiments, our approach lags behind DSNO (Zheng et al., 2022) and CD (Song et al., 2023), which achieves a lower FID of 7.83 and 6.20 respectively. Despite this, it is worth emphasizing that our method does not entail the additional costs associated with generating expensive synthetic data, which is a characteristic feature of DSNO. This cost-effective aspect represents a notable advantage of our approach in the context of ImageNet 64x64 experiments despite its poorer performance.

In Figure 2, we compare qualitatively between the images generated from the teacher EDM model and the student model. From this, we observe that in general, the student model aligns with the teacher model images, generating similar images for the same noise seed. Additional samples from Imagenet and CIFAR-10 are provided in Appendix A.4.

6 Abalation Study

6.1 Comparing Higher Order Numerical Differentiation

In this section, we investigate the impact of higher-order numerical differentiation on the distillation performance of PID. Specifically, we compare the outcomes of employing 1st order numerical differentiation with those obtained using the 2nd order Central Difference Method. While many higher-order approaches typically necessitate more than 2 model evaluations, leading to increased computational costs for numerical

Table 3: FID table comparisons for different order numerical differentiation on CIFAR 10.

Method	FID (↓)
PID (1st Order)	3.92
PID (2nd order - Central Difference)	3.68

gradient computation, the Central Difference method, despite being a second-order numerical differentiation technique, only requires 2 model evaluations, maintaining the same computational cost as the 1st order approach. As indicated in Table 3, the 2nd order approach exhibits a slightly superior performance compared to 1st order numerical differentiation. This aligns with observations from standard PINNs training, where higher-order numerical differentiation tends to yield solutions that closely align with the actual ODE system.

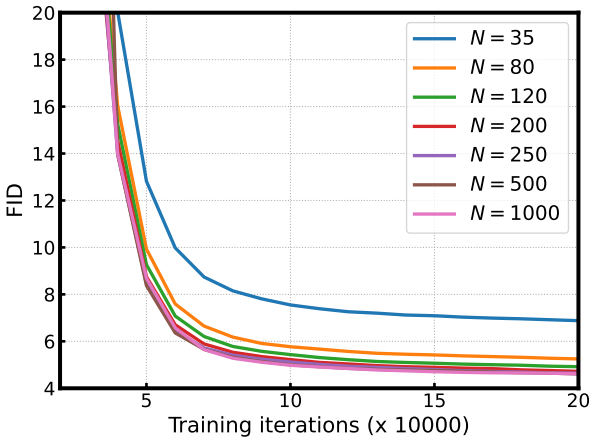

Figure 3: Training curve with different discretizations number on CIFAR-10.

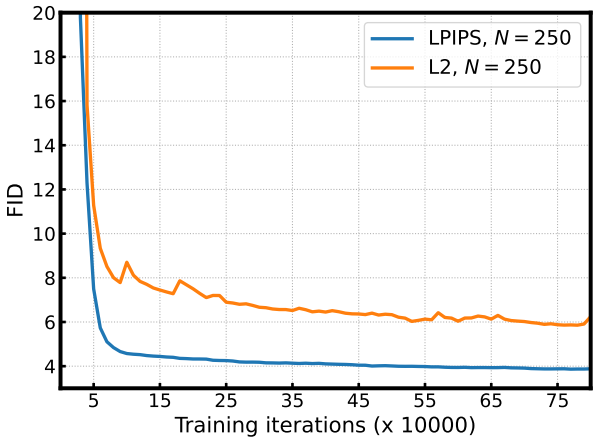

Figure 4: Training curve for different distance metrics, L2 and LPIPS, on CIFAR-10.

6.2 Comparing Discretization Numbers

To properly understand the effect of discretization number, N, on our method, the experiment on CIFAR-10 was repeated with different discretization values. The experiments conducted in this section were performed with the same hyperparameter setup as in the main results except with changing discritization number. The discretization values investigated here were $\{35, 80, 120, 200, 250, 500, 1000\}$.

In Figure 3, we can observe that the performance of our single step image generation model steadily increases with increasing discritization. This behaviour aligns well with the theoretical expectations according to Theorem 1 where the discritization error decreases with higher discritization. Additionally, this behaviour is also common to PINNs (Raissi et al., 2019) where increasing the collocation of points on a trajectory improves model performance. This stable and predictable trend with respect to discretization justifies our choice of setting our discritization number to 250 where the performance has plateaued, achieving good performance despite not tuning any methodology-specific hyperparameters.

6.3 L2 vs LPIPS comparison

To thoroughly investigate the influence of different distance metrics on model performance, we conducted experiments on CIFAR-10 using the L2 and LPIPS metrics. These experiments were carried out following the same experimental setup described in the main results. Analyzing the results depicted in Figure 4, we observe a similar trend to previous studies utilizing LPIPS metric (Song et al., 2023; Liu et al., 2022), wherein a slower convergence rate with L2 compared to LPIPS was observed. This difference between L2 and LPIPS persists even up till convergence with the L2 metric obtaining an FID of 5.85 and the LPIPS

metric achieving an FID of 3.92. Consequently, this reinforces the validity and suitability of the LPIPS metric in our training approach.

6.4 Training Efficiency Comparison

Due to the incorporation of numerical differentiation in our approach, we regrettably require two model evaluations, in contrast to the single model evaluations employed by other methods. In this section, we provide a detailed comparison of the training time efficiency of our method with recent works, CD (Song et al., 2023) and PD (Salimans & Ho, 2022). The analysis presented in Table 4 reveals an intriguing finding: despite the necessity of two functional evaluations, our approach incurs only a 35% higher training cost compared to doubling, as might be expected. This discrepancy arises from the fact that, while our method uses only a single teacher model evaluation, recent methods instead requires two iterative teacher model evaluations, thus incurring additional training expenses. It is worth emphasizing that despite the additional training cost per iteration attributed to our approach, the consistent and stable trend we observe concerning the discretization number allows us to train our model without the need to fine-tune any methodology-specific hyperparameters. This, in turn, significantly reduces the cost associated with hyperparameter optimization.

Table 4: Training time comparisons between PID and recent works on CIFAR 10.

Method	Training Time (seconds per 10 iterations)
PD	5.15
CD	5.21
PID (ours)	7.13

Table 5: FID table comparisons for small student model and large student model on CIFAR 10.

Model	Parameters	FID (↓)
Teacher (EDM)	55.7M	2.04
Student (PID)	55.7M	3.93
Student (PID)	13.9M	8.29

6.5 Knowledge Distillation

As is common in Knowledge Distillation literature, this field often involves model compression where a teacher model is used to produce a student model with comparable performance. In line with this paradigm, we train our model with the same hyperparameters as in the CIFAR-10 main results with less than a quarter of the model parameters. The small student architecture was constructed by reducing all the channels in the teacher models by half. More details on the small student architecture are provided in Appendix A.1. From Table 5, we can observe that despite the student model's significantly smaller size, it is still able to generate decent images, achieving an FID score of 8.29. Despite its drop in performance in contrast to the bigger student models, this result showcases the promising potential of Knowledge Distillation approaches in model compression and not just NFE reduction.

7 Conclusion

In this paper, we introduce Physics Informed Distillation (PID), a method designed to train a single-step diffusion model that draws significant inspiration from Physics Informed Neural Networks (PINNs). Through a combination of empirical evaluations and theoretical underpinnings, we have demonstrated the robustness and competitiveness of our method in comparison to the majority of existing techniques. While it falls slightly behind DSNO and CD, it distinguishes itself by eschewing the need for costly synthetic data generation or meticulous tuning of methodology-specific hyperparameters. Instead, our approach achieves competitive performance with constant methodology-specific hyperparameters.

References

Dmitry Baranchuk, Ivan Rubachev, Andrey Voynov, Valentin Khrulkov, and Artem Babenko. Label-efficient semantic segmentation with diffusion models. *arXiv preprint arXiv:2112.03126*, 2021.

Andrew Brock, Jeff Donahue, and Karen Simonyan. Large scale GAN training for high fidelity natural image synthesis. In *International Conference on Learning Representations*, 2019. URL `https://openreview.net/forum?id=B1xsqj09Fm`.

Mathilde Caron, Hugo Touvron, Ishan Misra, Hervé Jégou, Julien Mairal, Piotr Bojanowski, and Armand Joulin. Emerging properties in self-supervised vision transformers. In *Proceedings of the IEEE/CVF international conference on computer vision*, pp. 9650–9660, 2021.

Xinlei Chen, Haoqi Fan, Ross Girshick, and Kaiming He. Improved baselines with momentum contrastive learning. *arXiv preprint arXiv:2003.04297*, 2020.

Pao-Hsiung Chiu, Jian Cheng Wong, Chinchun Ooi, My Ha Dao, and Yew-Soon Ong. Can-pinn: A fast physics-informed neural network based on coupled-automatic–numerical differentiation method. *Computer Methods in Applied Mechanics and Engineering*, 2022.

Salvatore Cuomo, Vincenzo Schiano Di Cola, Fabio Giampaolo, Gianluigi Rozza, Maziar Raissi, and Francesco Piccialli. Scientific machine learning through physics–informed neural networks: where we are and what's next. *Journal of Scientific Computing*, 2022.

Jia Deng, Wei Dong, Richard Socher, Li-Jia Li, Kai Li, and Li Fei-Fei. Imagenet: A large-scale hierarchical image database. In *2009 IEEE conference on computer vision and pattern recognition*, 2009.

Prafulla Dhariwal and Alexander Nichol. Diffusion models beat gans on image synthesis. *Advances in Neural Information Processing Systems*, 2021.

Zhengyang Geng, Ashwini Pokle, and J Zico Kolter. One-step diffusion distillation via deep equilibrium models. In *Thirty-seventh Conference on Neural Information Processing Systems*, 2023. URL `https://openreview.net/forum?id=b6XvK2de99`.

Ian Goodfellow, Jean Pouget-Abadie, Mehdi Mirza, Bing Xu, David Warde-Farley, Sherjil Ozair, Aaron Courville, and Yoshua Bengio. Generative adversarial networks. *Communications of the ACM*, 2020.

Christopher Grant. Lecture 4: Picard-lindelöf theorem. `http://www.math.byu.edu/~grant/courses/m634/f99/lec4.pdf`, 1999.

Jean-Bastien Grill, Florian Strub, Florent Altché, Corentin Tallec, Pierre Richemond, Elena Buchatskaya, Carl Doersch, Bernardo Avila Pires, Zhaohan Guo, Mohammad Gheshlaghi Azar, et al. Bootstrap your own latent-a new approach to self-supervised learning. *Advances in neural information processing systems*, 33:21271–21284, 2020.

Jiatao Gu, Shuangfei Zhai, Yizhe Zhang, Lingjie Liu, and Joshua M Susskind. Boot: Data-free distillation of denoising diffusion models with bootstrapping. In *ICML 2023 Workshop on Structured Probabilistic Inference {\&} Generative Modeling*, 2023.

Martin Heusel, Hubert Ramsauer, Thomas Unterthiner, Bernhard Nessler, and Sepp Hochreiter. Gans trained by a two time-scale update rule converge to a local nash equilibrium. In I. Guyon, U. Von Luxburg, S. Bengio, H. Wallach, R. Fergus, S. Vishwanathan, and R. Garnett (eds.), *Advances in Neural Information Processing Systems*. Curran Associates, Inc., 2017a.

Martin Heusel, Hubert Ramsauer, Thomas Unterthiner, Bernhard Nessler, and Sepp Hochreiter. Gans trained by a two time-scale update rule converge to a local nash equilibrium. *Advances in neural information processing systems*, 2017b.

Jonathan Ho, Ajay Jain, and Pieter Abbeel. Denoising diffusion probabilistic models. *Advances in neural information processing systems*, 33:6840–6851, 2020.

Kurt Hornik, Maxwell Stinchcombe, and Halbert White. Multilayer feedforward networks are universal approximators. *Neural networks*, 1989.

Tero Karras, Miika Aittala, Timo Aila, and Samuli Laine. Elucidating the design space of diffusion-based generative models, 2022.

Diederik P Kingma and Max Welling. Auto-encoding variational bayes. *arXiv preprint arXiv:1312.6114*, 2013.

Durk P Kingma and Prafulla Dhariwal. Glow: Generative flow with invertible 1x1 convolutions. *Advances in neural information processing systems*, 2018.

Alexander Kirillov, Eric Mintun, Nikhila Ravi, Hanzi Mao, Chloe Rolland, Laura Gustafson, Tete Xiao, Spencer Whitehead, Alexander C Berg, Wan-Yen Lo, et al. Segment anything. *arXiv preprint arXiv:2304.02643*, 2023.

Alex Krizhevsky and Geoffrey Hinton. Learning multiple layers of features from tiny images. Technical Report 0, University of Toronto, Toronto, Ontario, 2009. URL `https://www.cs.toronto.edu/~kriz/learning-features-2009-TR.pdf`.

Isaac E Lagaris, Aristidis Likas, and Dimitrios I Fotiadis. Artificial neural networks for solving ordinary and partial differential equations. *IEEE transactions on neural networks*, 1998.

Haoying Li, Yifan Yang, Meng Chang, Shiqi Chen, Huajun Feng, Zhihai Xu, Qi Li, and Yueting Chen. Srdiff: Single image super-resolution with diffusion probabilistic models. *Neurocomputing*, 2022.

Liyuan Liu, Haoming Jiang, Pengcheng He, Weizhu Chen, Xiaodong Liu, Jianfeng Gao, and Jiawei Han. On the variance of the adaptive learning rate and beyond. In *International Conference on Learning Representations*, 2020. URL `https://openreview.net/forum?id=rkgz2aEKDr`.

Xingchao Liu, Chengyue Gong, and Qiang Liu. Flow straight and fast: Learning to generate and transfer data with rectified flow. *arXiv preprint arXiv:2209.03003*, 2022.

Cheng Lu, Yuhao Zhou, Fan Bao, Jianfei Chen, Chongxuan Li, and Jun Zhu. Dpm-solver: A fast ode solver for diffusion probabilistic model sampling in around 10 steps. *arXiv preprint arXiv:2206.00927*, 2022.

Eric Luhman and Troy Luhman. Knowledge distillation in iterative generative models for improved sampling speed. *arXiv preprint arXiv:2101.02388*, 2021.

Weijian Luo, Tianyang Hu, Shifeng Zhang, Jiacheng Sun, Zhenguo Li, and Zhihua Zhang. Diff-instruct: A universal approach for transferring knowledge from pre-trained diffusion models. In *Thirty-seventh Conference on Neural Information Processing Systems*, 2023. URL `https://openreview.net/forum?id=MLIs5iRq4w`.

Alex Nichol, Prafulla Dhariwal, Aditya Ramesh, Pranav Shyam, Pamela Mishkin, Bob McGrew, Ilya Sutskever, and Mark Chen. Glide: Towards photorealistic image generation and editing with text-guided diffusion models. *arXiv preprint arXiv:2112.10741*, 2021.

Axi Niu, Kang Zhang, Trung X Pham, Jinqiu Sun, Yu Zhu, In So Kweon, and Yanning Zhang. Cdpmsr: Conditional diffusion probabilistic models for single image super-resolution. *arXiv preprint arXiv:2302.12831*, 2023.

Maziar Raissi, Paris Perdikaris, and George E Karniadakis. Physics-informed neural networks: A deep learning framework for solving forward and inverse problems involving nonlinear partial differential equations. *Journal of Computational physics*, 2019.

Aditya Ramesh, Prafulla Dhariwal, Alex Nichol, Casey Chu, and Mark Chen. Hierarchical text-conditional image generation with clip latents. *arXiv preprint arXiv:2204.06125*, 2022.

Chitwan Saharia, William Chan, Saurabh Saxena, Lala Li, Jay Whang, Emily L Denton, Kamyar Ghasemipour, Raphael Gontijo Lopes, Burcu Karagol Ayan, Tim Salimans, et al. Photorealistic text-to-image diffusion models with deep language understanding. *Advances in Neural Information Processing Systems*, 2022a.

Chitwan Saharia, Jonathan Ho, William Chan, Tim Salimans, David J Fleet, and Mohammad Norouzi. Image super-resolution via iterative refinement. *TPAMI*, 2022b.

Tim Salimans and Jonathan Ho. Progressive distillation for fast sampling of diffusion models. *arXiv preprint arXiv:2202.00512*, 2022.

Tim Salimans, Ian Goodfellow, Wojciech Zaremba, Vicki Cheung, Alec Radford, and Xi Chen. Improved techniques for training gans. *Advances in neural information processing systems*, 2016.

Karen Simonyan and Andrew Zisserman. Very deep convolutional networks for large-scale image recognition. *arXiv preprint arXiv:1409.1556*, 2014.

Jascha Sohl-Dickstein, Eric Weiss, Niru Maheswaranathan, and Surya Ganguli. Deep unsupervised learning using nonequilibrium thermodynamics. In *International Conference on Machine Learning*, 2015.

Jiaming Song, Chenlin Meng, and Stefano Ermon. Denoising diffusion implicit models. *arXiv preprint arXiv:2010.02502*, 2020a.

Yang Song, Jascha Sohl-Dickstein, Diederik P Kingma, Abhishek Kumar, Stefano Ermon, and Ben Poole. Score-based generative modeling through stochastic differential equations. *arXiv preprint arXiv:2011.13456*, 2020b.

Yang Song, Jascha Sohl-Dickstein, Diederik P. Kingma, Abhishek Kumar, Stefano Ermon, and Ben Poole. Score-based generative modeling through stochastic differential equations, 2021.

Yang Song, Prafulla Dhariwal, Mark Chen, and Ilya Sutskever. Consistency models. *arXiv preprint arXiv:2303.01469*, 2023.

George E Uhlenbeck and Leonard S Ornstein. On the theory of the brownian motion. *Physical review*, 1930.

Ming Chen Wang and George Eugene Uhlenbeck. On the theory of the brownian motion ii. *Reviews of modern physics*, 1945.

Jay Whang, Mauricio Delbracio, Hossein Talebi, Chitwan Saharia, Alexandros G Dimakis, and Peyman Milanfar. Deblurring via stochastic refinement. In *CVPR*, 2022.

Julia Wolleb, Robin Sandkühler, Florentin Bieder, Philippe Valmaggia, and Philippe C Cattin. Diffusion models for implicit image segmentation ensembles. In *International Conference on Medical Imaging with Deep Learning*, 2022.

Zhantao Yang, Ruili Feng, Han Zhang, Yujun Shen, Kai Zhu, Lianghua Huang, Yifei Zhang, Yu Liu, Deli Zhao, Jingren Zhou, et al. Eliminating lipschitz singularities in diffusion models. *arXiv preprint arXiv:2306.11251*, 2023.

Qinsheng Zhang and Yongxin Chen. Fast sampling of diffusion models with exponential integrator. *arXiv preprint arXiv:2204.13902*, 2022.

Hongkai Zheng, Weili Nie, Arash Vahdat, Kamyar Azizzadenesheli, and Anima Anandkumar. Fast sampling of diffusion models via operator learning. *arXiv preprint arXiv:2211.13449*, 2022.

A Appendix

A.1 Additional Experiment details

Model Architectures All pre-trained models utilized in our experiments were obtained from the EDM framework (Karras et al., 2022). Specifically, for the CIFAR-10 dataset, we employed the NCSN++ model architecture as described by (Song et al., 2021). For experiments conducted on the ImageNet 64x64 dataset, we followed the architecture detailed by (Dhariwal & Nichol, 2021). For small student distillation experiment on CIFAR-10, the same architecture as the teacher model in (Song et al., 2021) was used with the number of channels reduced from 128 to 64.

Evaluation Metrics For Frechet inception distance (FID, lower is better) (Heusel et al., 2017a) and Inception Score (IS, higher is better) (Salimans et al., 2016), 50,000 generated images were compared against their respective ground truth datasets. Three different seeds were employed, and the best result was selected since FID values typically exhibit approximately 2% variance between measurements (Karras et al., 2022).

Training details For both CIFAR-10 and ImageNet, we use a pretrained EDM model (Karras et al., 2022) as our teacher model. Unless stated otherwise, all the student models $\mathbf{X}_\theta$ were initialized with the same weight as the pretrained EDM teacher model D_ϕ. In the experiment involving the smaller student model, the student model was randomly initialized. Rectified Adam optimizer (Liu et al., 2020) was used for distillation with weight decay of 0 and a constant learning rate throughout the training iteration. Following (Karras et al., 2022), we use the EMA weights of student model for inference. The EMA decay value for both CIFAR-10 and ImageNet is same, 0.99995. Additional details on training hyperparameters are shown in Table 6.

Unless explicitly stated otherwise, we utilized LPIPS as the default distance metric for training. When utilizing LPIPS as the distance metric $d(\cdot, \cdot)$, the input images were rescaled to 244x244 using bilinear upsampling before being fed into the VGG model (Simonyan & Zisserman, 2014).

Table 6: Hyperparameters used for the training runs.

Hyperparameter	CIFAR-10	ImagetNet 64x64
Number of GPUs	8xA100	32xA100
Batch size	512	2048
Gradient clipping	-	✓
Mixed-precision (FP16)	-	✓
Learning rate $\times 10^{-4}$	2	1
Dropout probability	0%	0%
EMA student model	0.99995	0.99995

A.2 Insight on Parametrization Choice for Physics Informed Distillation

To satisfy the boundary condition, we require a parametrization choice such that:

$$\begin{aligned} \mathbf{x}_\theta(\mathbf{z}, t) =& c_{\text{skip}}(t)\ \mathbf{z} + c_{\text{out}}(t)\ \mathbf{X}_\theta\left(c_{\text{in}}(T)\ \mathbf{z}, c_{\text{noise}}(t)\right), \\ & \text{where } c_{\text{out}}(T) = 0. \end{aligned} \tag{14}$$

A straightforward selection for this would be a linear function, such as $T - t$. However, for cases where T of the forward diffusion process is large, as in the case of EDM (Karras et al., 2022), such a choice would amplify the model outputs which may cause poor performance. As such, we choose:

$$c_{\text{out}}(t) = \frac{T - t}{T} \tag{15}$$

to ensure that the model is multiplied by a factor no larger than 1. For the skip connection function, $c_{\text{out}}(t)$, let's begin by examining the solution for the provided Probability Flow ODE system:

$$\mathbf{x}_t = \mathbf{z} + \int_T^t \frac{\mathbf{x}'_t - D_\phi(\mathbf{x}'_t, t')}{t'} \, \mathrm{d}t'. \tag{16}$$

Given that the constant function, $c_{\text{skip}}(t) = 1$, already meets its boundary condition at T, it might appear to be the obvious choice for the skip function. However, when considering Equation 16 and Equation 14, it can be seen that the model, $\mathbf{X}_\theta$, when it solves the ODE system is such that:

$$\begin{aligned} \mathbf{X}_\theta(\mathbf{z}, t) =& \frac{1}{c_{\text{out}}(t)} \int_T^t \frac{\mathbf{x}'_t - D_\phi(\mathbf{x}'_t, t')}{t'} \, \mathrm{d}t' \\ =& \frac{T}{T-t} \int_T^t \frac{\mathbf{x}'_t - D_\phi(\mathbf{x}'_t, t')}{t'} \, \mathrm{d}t'. \end{aligned} \tag{17}$$

At time $t = 0$,

$$\begin{aligned} \mathbf{X}_\theta(\mathbf{z}, 0) &= \int_T^0 \frac{\mathbf{x}'_t - D_\phi(\mathbf{x}'_t, t')}{t'} \, \mathrm{d}t' \\ &= \mathbf{x}_0 - \mathbf{z}. \end{aligned} \tag{18}$$

Given the contrasting magnitudes of $\mathbf{x}_0$ within the range $[-1, 1]$ and $\mathbf{z}$ which has significantly larger values due to its high variance, aligning our model, $\mathbf{X}_\theta(\mathbf{z}, 0)$, with $\mathbf{x}_0$ at $t = 0$ emerges as a superior choice. More specifically:

$$\begin{aligned} \mathbf{X}_\theta(\mathbf{z}, 0) &= \mathbf{x}_0 \\ &= \mathbf{z} + \int_T^0 \frac{\mathbf{x}'_t - D_\phi(\mathbf{x}'_t, t')}{t'} \, \mathrm{d}t'. \end{aligned} \tag{19}$$

Thus, for any arbitrary time, t, we desire our model to be expressed as:

$$\mathbf{X}_\theta(\mathbf{z}, t) = \mathbf{z} + \frac{T}{T-t} \int_T^t \frac{\mathbf{x}'_t - D_\phi(\mathbf{x}'_t, t')}{t'} \, \mathrm{d}t'. \tag{20}$$

By plugging in the above formula into Equation 14, considering the choice of c_{out} as well as the solution of the probability flow ODE in Equation 16, we obtain the given skip connection:

$$c_{\text{skip}}(t) = \frac{t}{T} \tag{21}$$

For the choice of functions, $c_{\text{in}}(t)$ and $c_{\text{noise}}(t)$, we opted to use the same functions utilized in the teacher EDM model. Additionally, the time value of the in function, $c_{\text{in}}(T)$, is set to T, given that the input consists of noise, representing the distribution corresponding to time T.

A.3 Trajectory comparisons

In Figure 5, we present a comparison of the trajectories obtained from both the teacher EDM model and the student PID model. Notably, for the same noise seed, we observe that the trajectories represented by $x_\theta(\mathbf{z}, \cdot)$ in the student model align remarkably well with those of the teacher model, with only minor aberrations. This demonstration underscores the ability of our model to predict all points along the trajectory in a continuous manner and not only the origin.

A.4 Additional Random Samples

In this section, we provide additional samples from our PID model for ImageNet 64x64 and CIFAR-10. The images are obtained by employing the same class for ImageNet 64x64 and applying the same noise seed to both the teacher EDM and student PID models.

Figure 5: Trajectory comparisons on ImageNet with EDM teacher (top) and PID student (bottom).

A.4.1 CIFAR-10

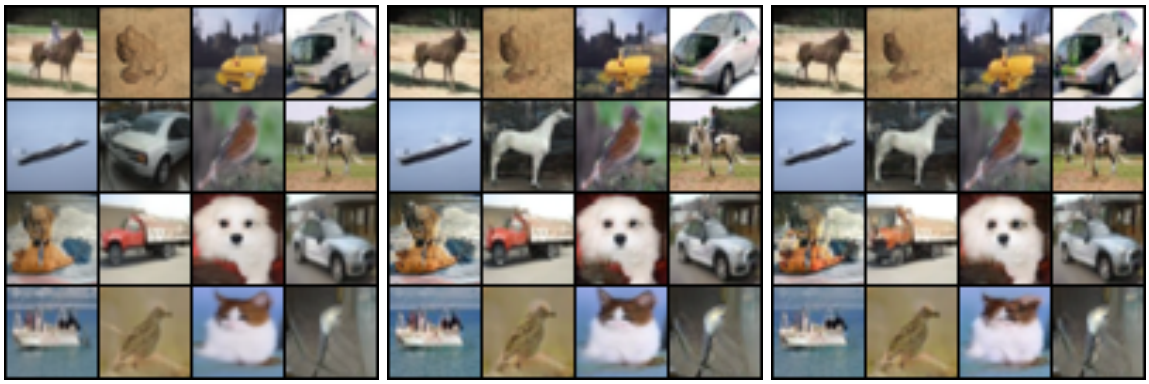

(a) Random samples from EDM (b) Random samples from PID (c) Random samples from PID (small student)

Figure 6: Unconditional image generation comparison on CIFAR-10 for the same seed. Left panel: random samples generated by EDM teacher model. Middle panel: generated by PID student model. Right panel: generated by small PID student model.

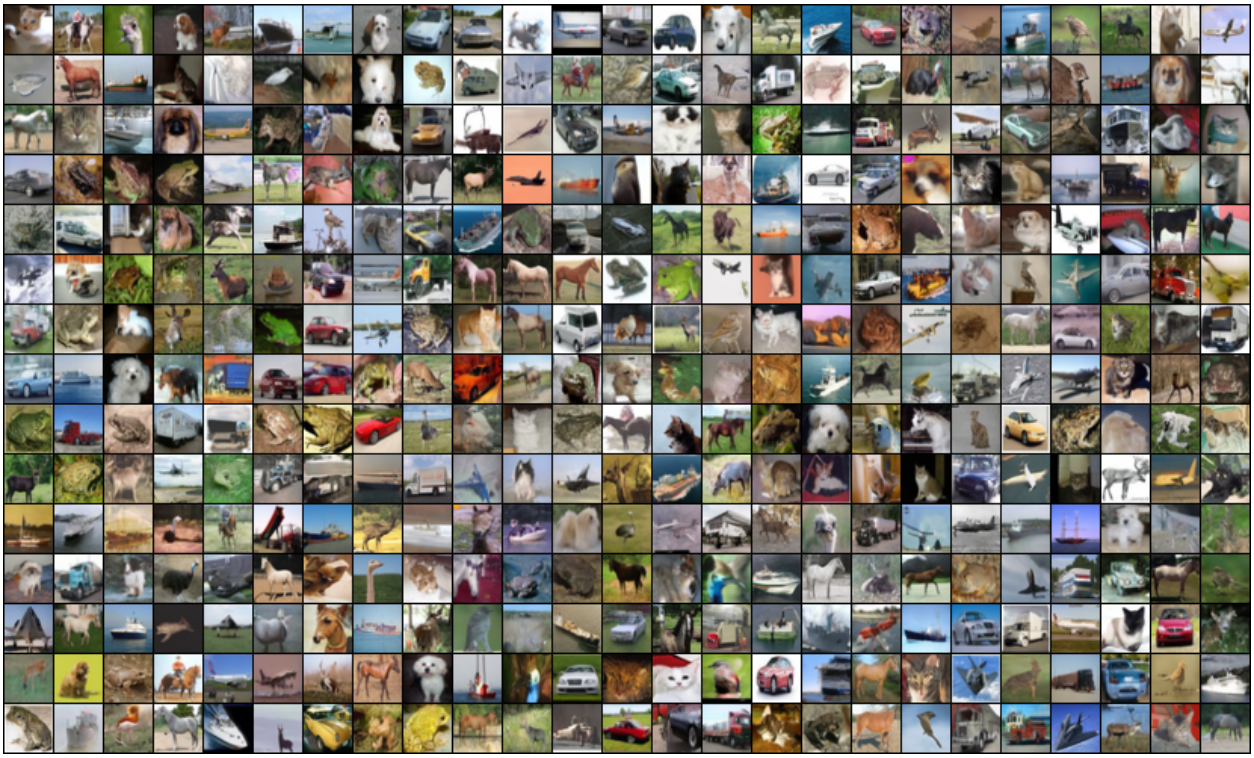

(a) Random samples from EDM (FID=2.04)

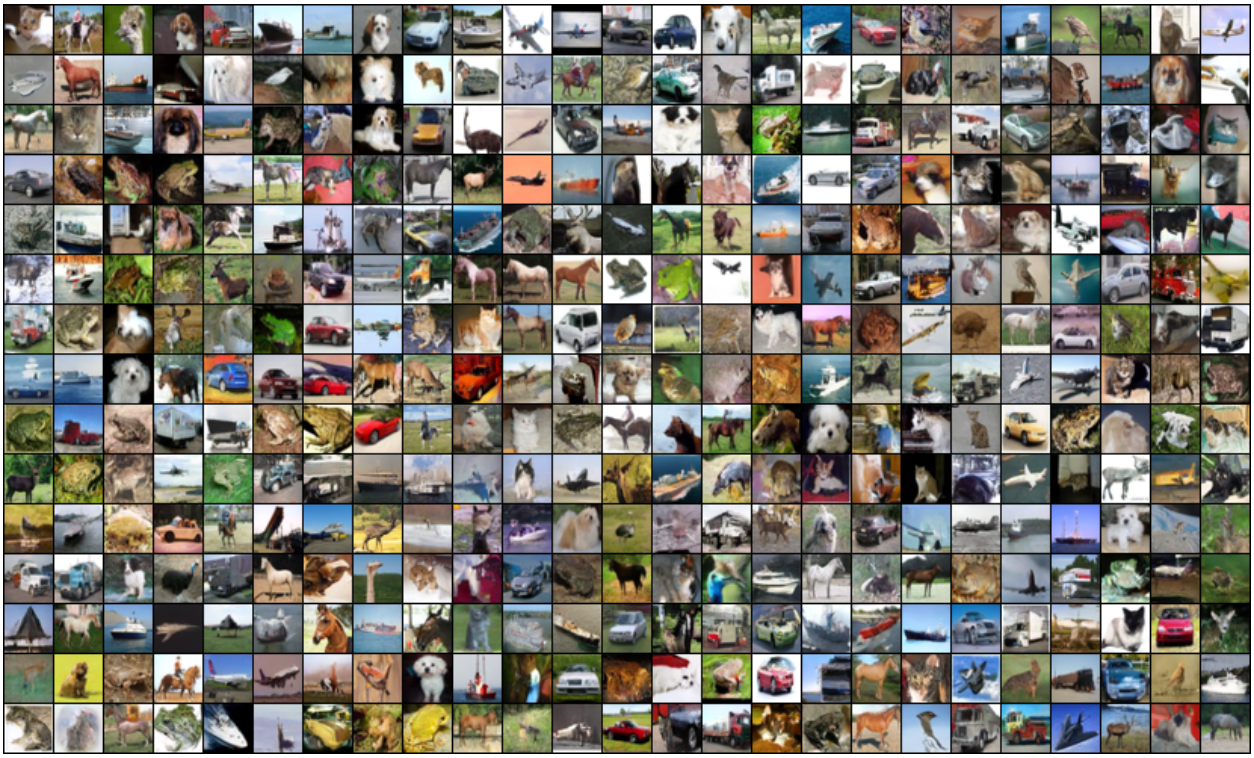

(b) Random samples from PID (FID=3.92)

(c) Random samples from PID small student (FID=8.29)

Figure 7: Unconditional image generation comparison on CIFAR-10 for the same seed.

A.4.2 ImageNet 64x64

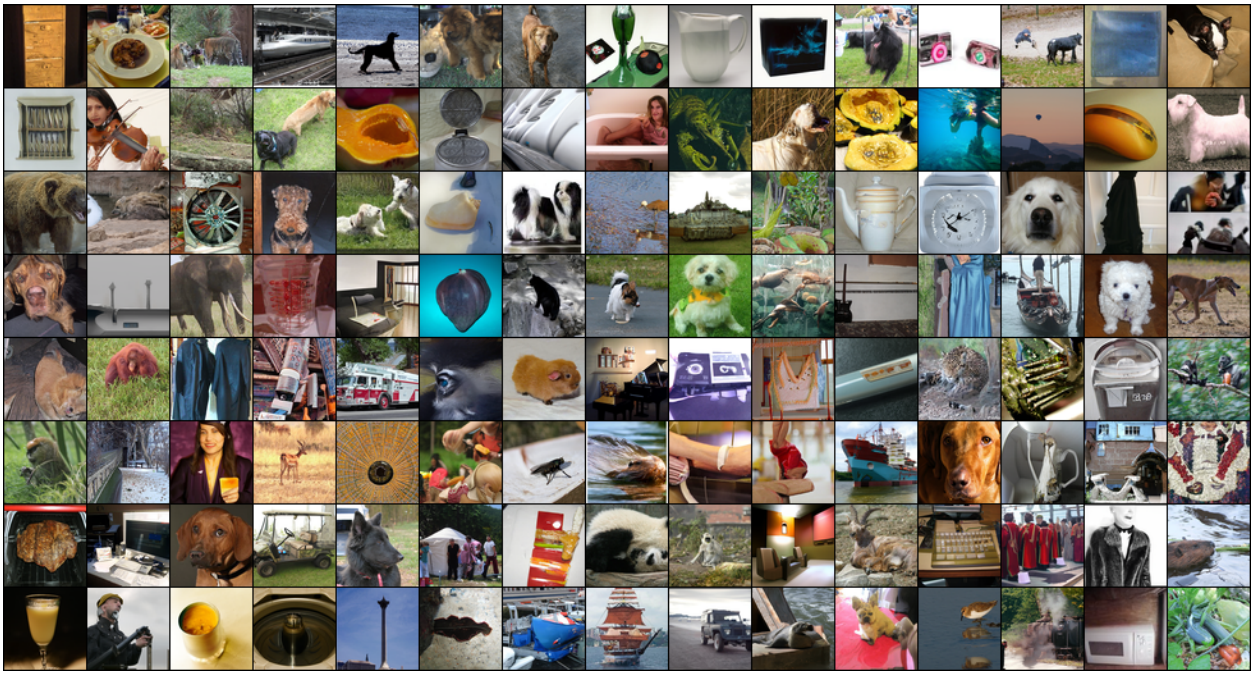

(a) Random samples from EDM on ImageNet (FID=2.44)

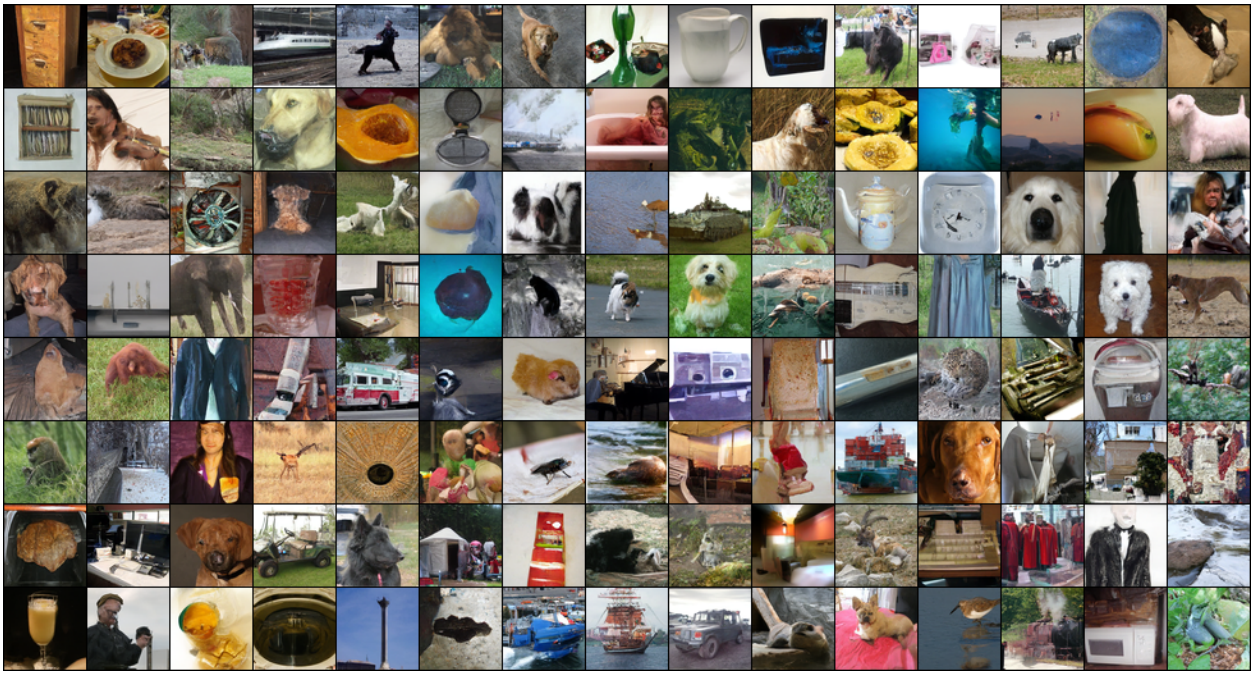

(b) Random samples from PID on ImageNet (FID=9.49)

Figure 8: Conditional image generation comparison on ImageNet 64×64 for the same seed.